Asian Journal of Chemistry; Vol. 28, No. 7 (2016), 1486-1492

ASIAN JOURNAL OF CHEMISTRY

http://dx.doi.org/10.14233/ajchem.2016.19726

Synthesis, Characterization and Catalytic Activity of Manganese(II)-Cobalt(II) Complexes Anchored SBA-16 for Liquid Phase Oxidation of *p*-Xylene

PHAM XUAN NUI[1,*], NGUYEN NHO DUNG[2] and TRAN THI VAN THI[2]

[1]Department of Chemical Engineering, Hanoi University of Mining and Geology, Duc Thang, Tu Liem North, Hanoi, Vietnam
[2]Department of Chemistry, Hue Science College, Hue University,77 Nguyen Hue Street, Hue City, Vietnam

*Corresponding author: Fax: +84 438389633; Tel: +84 912278942; +84 984273379; E-mail: phamxuannui@gmail.com

Received: 12 November 2015; *Accepted*: 1 January 2016; *Published online*: 31 March 2016; AJC-17834

In this study, the results of synthesis and modified mesoporous surface of SBA-16 by using Schiff-base complexes [Co(II)-Mn(II)-Sal-APTES] were presented. Manganese(II) and cobalt(II)-Schiff bases complexes were synthesized by reaction between salicylaldehyde (Sal) and 3-aminopropyl triethoxy silane (APTES) in ethanol solution to form Schiff-base ligands. The Co(II)-Mn(II)-Sal-APTES-SBA-16 catalysts were analyzed by a series of analytical methods such as UV-Vis-DRS,XRD, N_2 sorption isotherm, FT-IR, TGA-DTA, XPS and TEM. The results showed that the synthesized catalyst remains the pore size of SBA-16 after the covalent anchoring of Co(II)-Mn(II)-Sal-APTES complex over SBA-16 support. This catalyst was examined in the liquid phase oxidation of *p*-xylene using H_2O_2 as an oxidant. The catalytic activity was examined by the liquid phase oxidation of *p*-xylene using H_2O_2 as an oxidant. It was found that catalyst show higher catalytic activity for the liquid phase oxidation of *p*-xylene. The combination of cobalt(II) and manganese(II) complexes to afford Co(II)-Mn(II)-APTES-SBA-16 catalyst enhances the response performance and product selectivity significantly oriented to terephthalic acid product.

Keywords: Surfaces, Co(II)-Mn(II)-Sal-APTES, Thermogravimetric analysis, X-ray diffraction, Catalytic properties.

INTRODUCTION

The oxidation products (alcohols, aldehydes, ketones, acids, *etc*.) from petrochemical technology, are important to industrial applications. They have been used to produce pigments, pharmaceuticals, plasticized compounds, agricultural chemicals, silks and plastics in electronic equipment and many other implements [1]. Terephthalic acid (TPA) and dimethyl terephthalic acid are the raw materials for polyester production to produce textile [2]. Currently, terephthalic acid has been produced by the liquid phase catalytic oxidation of *p*-xylene [3-6] with the homogenous catalyst consisting of cobalt acetate, manganese acetate, which are soluble in acetic acid in the presence of hydrobromic acid. In fact, these oxidations still use the homogeneous catalysts such as complexed solution of metal. The advantage of using homogenous catalyst is able to get high yield reaction under low temperature and pressure [7]. However, using homogenous catalysts is limited because it is difficult to separate products after reaction, that their stability is not high and they pose a threat to the environment. There have been a general strategy is to use heterogeneous catalysts which contains the covalent anchoring using Schiff-base complexes for the sustainable development [8,9]. In addition, the Schiff-base complexes have been widely used as catalyst for liquid phase oxidation because they are low-cost, synthesized by using a simple process, are their high structural and thermal stability [10].

Recently, using a new type of catalyst, named pseudo-heterogeneous catalyst which possessed both benefits of homogenous and heterogeneous catalysts has gained much attention from scientists. Chaube *et al.* [11] have synthesized Mn(III) and Co(II)-salen complexes immobilized over mesoporous alumina and used this catalyst for the liquid phase oxidation of styrene and cyclohexene, while Sharma *et al.* [12] synthesized the Mn(II)-based binaphthyl Schiff complex over organo-modified SBA-15 by using chloro(S,S)(-)[N-3-*tert*-butyl-5-chloromethyl salicylidene]-N'-[3',5'-di-*tert*-butyl salicylidene]1,1'-binaphthyl-2,2'-diamino manganese(III). The Pd(II) Schiff-base complex was prepared by the reaction of salicylaldehyde and (3-aminopropyl)trimethoxysilane in methanol and subsequent complexation with $Pd(OAc)_2$ as a novel nanocatalyst for the synthesis of 2,3-disubstituted quinoxalines and pyridopyrazine derivatives [13]. Jacob *et al.* [14] studied oxidation of *p*-xylene over zeolite-encapsulated copper and manganese complexes in aerobic condition. The halogen promoter as the initiator is not required,

however, low reaction conversion was obtained with only 50-60 wt %.

In this research, we studied a cobalt(II)-manganese(II) complex which binds to SBA-16 surface by 3-aminopropyl trimethyoxy silane to give supported catalyst and using this catalyst for the liquid phase oxidation of *p*-xylene.

EXPERIMENTAL

Pluronic F127 ($EO_{106}PO_{70}EO_{106}$), tetraethyl orthosilicate (TEOS), cobalt acetate, manganese acetate, salicylaldehyde, (3-aminopropyl)trimethoxysilane (APTES), HCl, glacial acetic acid, propan-1-ol and *p*-xylene were purchased from Sigma-Aldrich and Merck companies.

Preparation of SBA-16: SBA-16 was synthesized from the tetraethyl orthosilicate (TEOS) and F127 ($EO_{106}PO_{70}EO_{106}$) as precursors and using the hydrothermal method which was described by Gobin *et al.* [15]. In this synthesis, 4 g F_{127} dissolved in 200 mL of distilled water was stirred for 1 h. Then, 8.3 g of 12 M HCl was added, stirring continuously for 2 h at room temperature to obtain the homogenous mixture. After that, 12 g *n*-butanol was added in the mixture, reaction at 45 °C for 1 h. Finally, 20 g of TEOS was added slowly to yield a gel mixture, continuously stirring at 45 °C for 24 h. The mixture was then heated under the static condition at 100 °C for another 24 h in a autoclave. The solid product was separated by filtration repeatedly washed with distilled water and ethanol, then dried in an oven at 100 °C for 24 h and then calcined in the air at 550 °C for 6 h obtain the SBA-16 powder.

Synthesis of M(II)-Sal-APTES complex: Solution of salicylaldehyde (Sal) (1 mmol) and 3-aminopropyl trithoxy silane (APTES) (1 mmol) was stirred for 3 h at room temperature. A yellow solution was obtained due to the formation of the imine (C=N) group of compound (**Scheme-I**). Subsequently, the corresponding metal acetate *e.g.*, $Co(OAc)_2$ or $Mn(OAc)_2$ was added slowly to a solution of Sal-APTES and continuously stirring for 3 h at room temperature. Upon cooling complex solution, crystalline solid was separated. The solid product was separated by filtration washed with ethanol and then water. The metal complexes were recrystallized with heating by hot ethanol several times. The Co(II)-Mn(II)-Sal-APTES complex was obtained (**Scheme-II**) with molar ratio of M(II):Sal-APTES = 1:2.

Synthesis of M(II)-Sal-APTES-SBA-16 catalyst: Synthesis of M(II)-Sal-APTES-SBA-16 catalyst was performed by dispersion of M(II)-Sal-APTES onto SBA-16 support. SBA-16 was suspended in the ethanolic solution containing M(II)-Sal-APTES complex and were continuously stirred for 24 h at room temperature under inert atmosphere. After removal of solvents using a rotary evaporator, the green solid dried at 80 °C for 12 h, washed several times with ethanol and water to remove the free complex which the non-convalently grafted complex on surface of silica support. Finally product was dried at 80 °C for 8 h. The M(II)-Sal-APTES complex anchored onto SBA-16 was prepared according to **Scheme-III**.

Characterization of catalysts: Powder X-ray diffraction patterns were recorded on a D8-Advance Bruker with CuK_α radiation ($\lambda = 1.5406$ nm). N_2 adsorption-desorption isotherms were obtained on a Micromeritics Tristar 3000 sorptometer.

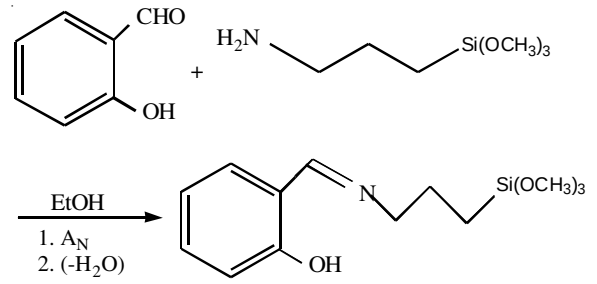

Scheme-I: Synthesis of the Schiff bases

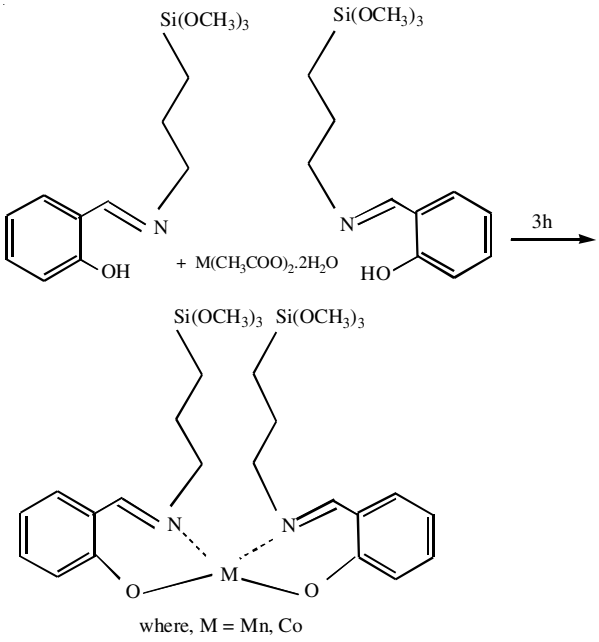

Scheme-II: Synthesis of Co(II) and Mn(II) complexes

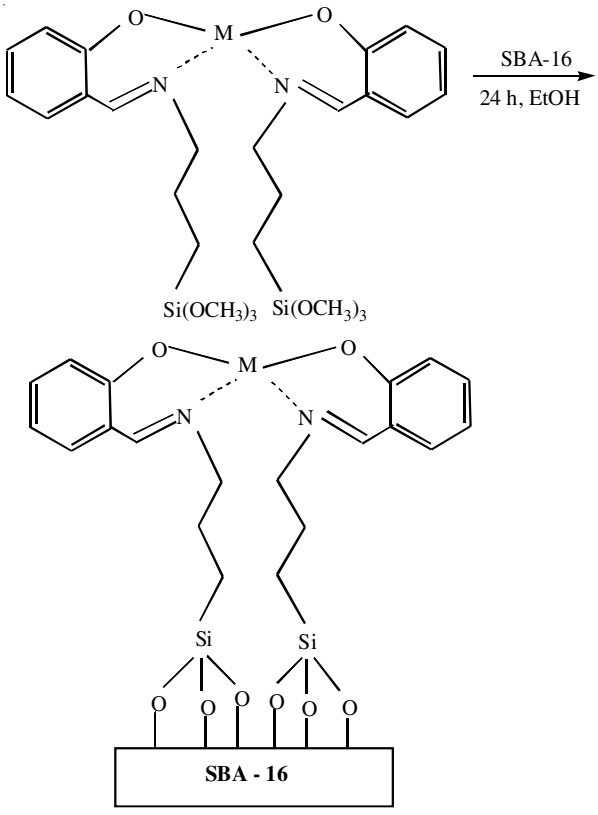

Scheme-III: Synthesis of M(II)-Sal-APTES-SBA-16; M is Co or Mn

Prior to analysis, the samples were outgassed at 180 °C in 6 h. BET surface areas were calculated from the linear part of the BET plot. Pore size distributions were calculated using the adsorption branches of the N_2 isotherms and the Barret-Joyner-Halenda (BJH) method. The images of transmission electron microscopy (TEM) were taken using a Hitachi S4800, operating at an accelerating voltage of 200 kV. Infrared data were examined on KBr pallets using a Shimadzu IR Prestige-21 spectrometer (Japan). Thermal gravimetricand differential thermal analysis (TG-DTA) were performed with a TG Setaram instrument (France) in the air of argon (100-1000 °C). UV-visible and UV-visible-Diffuse reflectance spectra were collected on a DR-Jasco V630 or a UV-Vis DRS-Jasco V670 spectrophotometer that was equipped with a diffuse reflectance attachment in which $BaSO_4$ was as the reference. XPS spectra were taken on an AXISULTRA DLD Shimadzu Kratos spectrometer (Japan) using monochromated Al K_α radiation (1486.6 eV).

Catalytic oxidation of *p*-xylene in liquid phase: Oxidation reaction of *p*-xylene was carried out as follow: 20 mL of *p*-xylene and precisely weighed catalyst were added into a 100 mL tree-neck round bottomed flask fitted with a water condenser and kept in water bath with continuous stirring. Hydrogen peroxide was dropped into the flask at a rate while the temperature was kept at a defined value.The contents of hydrogen peroxide were determined by iodometric method. After the reaction, the mixture was quenched to room temperature and then catalyst was filtered off.

The oxidation products of *p*-xylene were identified by GC-MS 7890A-5975C with a (30 m × 250 μm × 0.25 μm) HP-5MS column, 45-250 °C (45 °C in 2 min, 4 °C/min to 200 °C, 15 °C/min to 250 °C and kept in 5 min) and by LC-MS co-injection of standard compound. They were quantified by LC-MS Series 2A Shimadzu (Japan) with UV 254 nm) detector and SPD-10ADVP column, eluent consisting of 1 % acetic acid : acetonitrile with ratio 20:80 to 40:60 (w/w); with flow rate of 1 mL to 1.5 mL min^{-1}. The *p*-xylene conversion was determined as (moles of reacted *p*-xylene)/(moles of initial *p*-xylene) × 100 %. The selectivity of product (terephthalic acid-TA) was determined as (moles of the product)/(moles of reacted *p*-xylene) × 100 %.

RESULTS AND DISCUSSION

UV-visible-DRS spectra of M(II)-Sal-APTES complex: These experimental data indicate the formation of the Mn-ligand and/or the Co-ligand bond and the metal-Schiff base complexes were producted:

$$o\text{-HO-C}_6\text{H}_4\text{-CHO} + \text{H}_2\text{N-(CH}_2)_3\text{-Si(OC}_2\text{H}_5)_3 \rightarrow o\text{-HO-C}_6\text{H}_4\text{-CH=N-(CH}_2)_3\text{-Si(OC}_2\text{H}_5)_3 + \text{H}_2\text{O} \quad (1)$$

$$2o\text{-HO-C}_6\text{H}_4\text{-CH=N-(CH}_2)_3\text{-Si(OC}_2\text{H}_5)_3 + \text{M(CH}_3\text{COO)}_2 \rightarrow \text{M[O-C}_6\text{H}_4\text{-CH=N-(CH}_2)_3\text{-Si(OC}_2\text{H}_5)_3]_x + 2\,\text{CH}_3\text{COOH} \quad (2)$$

where M = Co or Mn.

Both metal complexes Mn-Sal-APTES (dark blue crystals) and Co-Sal-APTES (light green crystals) complex was defined by melting point of 126.8 ± 0.5 and 84.7 ± 0.5 °C, respectively. The maximum absorption wavelength of Mn-Sal-APTES was 415 nm (n-π*) and those of Co-Sal-APTES were 258 (π-π*), 387 (n-π*) in UV-visible spectra (Table-1). These values were different from those of previous chemicals. The electronic spectra of these complexes were taken in ethanol and the results is given in Fig. 1.

TABLE-1
UV-VISIBLE AND UV-VISIBLE-DRS DATA OF COMPOUNDS BEFORE AND AFTER COMPLEXED REACTION

Compounds	λ_{max} (nm) in ethanol
Sal-APTES ligand*	260 (π-π*), 320, 400 (n-π*)
$Co(OAc)_2$	520
Co(II)-Sal-APTES complex** (UV-visible and UV-visible-DRS)	258 (π-π*), 394 (n-π*)
$Mn(OAc)_2$	420
Mn(II)-Sal-APTES complex** (UV-visible and UV-visible-DRS)	415

*Sal: APTES ratio = 1:1 (mmol)
**$M(OAc)_2 \cdot 4H_2O$:Sal:APTES ratio = 0.5:1:1 (mmol)

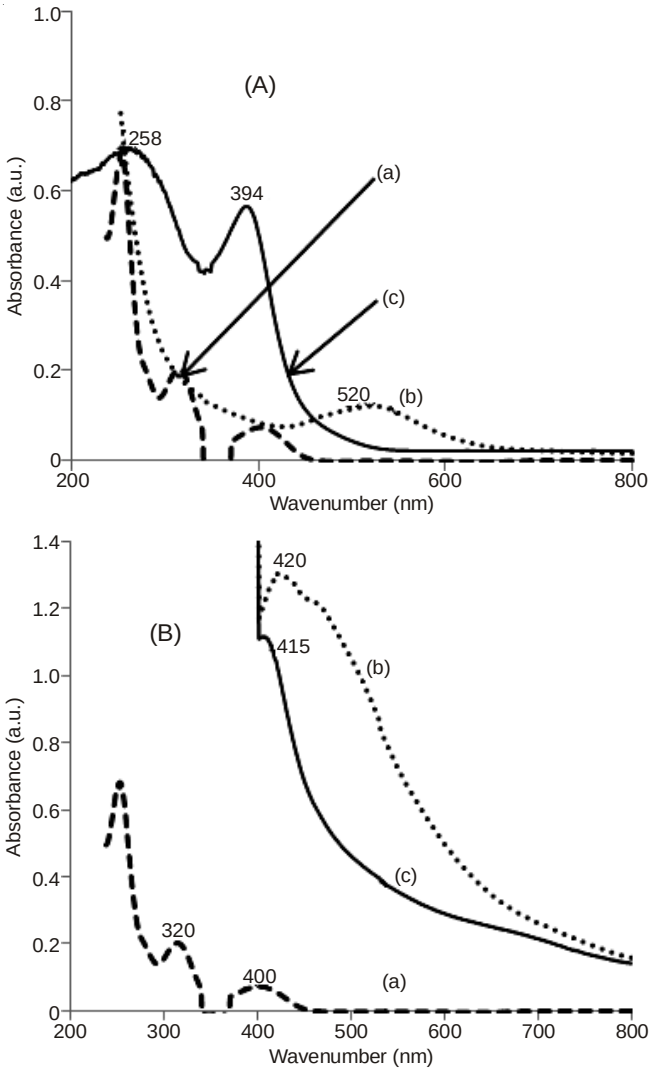

Fig. 1. UV-visible-DRS spectra of: (a) Sal-APTES, (b) neat $M(OAc)_2$, (c) M(II)-Sal-APTES, M: (A) Co, (B) Mn

FT-IR spectra: Fig. 2 shows the FT-IR spectra of SBA-16, Mn(II)-Sal-APTES-SBA-16, Co(II)-Sal-APTES-SBA-16 and Co(II)-Mn(II)-Sal-APTES-SBA-16 catalysts. The results show that the bands associated with both the support and with the Schiff-base complex. For the SBA-16 support have a strong

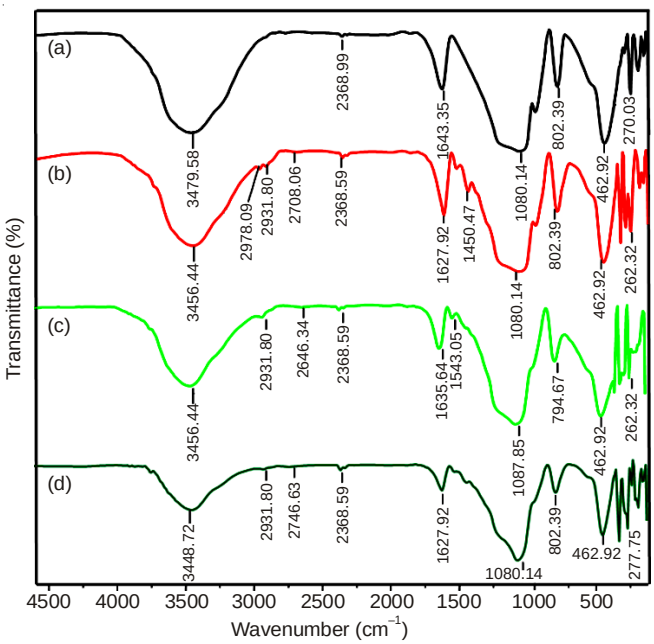

Fig. 2. FT-IR spectra of (a) SBA-16; (b) Mn(II)-Sal-APTES-SBA-16; (c) Co(II)Sal-APTES-SBA-16; and (d) Co(II)-Mn(II)-Sal-APTES-SBA-16

peak for stretching vibrations of (Si-O)in 802-794 cm^{-1} regions and the stretching band 1080 cm^{-1} is assigned to the asymmetric (Si-O-Si) vibrations. Specially, the as-synthesized samples exhibited the weak absorption bands from 2978 to 2931 cm^{-1} and ν at 1543 to 1450 cm^{-1}corresponding to the C-C stretching and (-CH_2) vibrations of the methoxy (-OCH_3)$_3$ groups and the propyl in the surfactant molecules. Further, the IR spectrum which characterize for free -NH_2 group in the APTES disappears in the spectrum of complex, in addition to some new peaks which charaterize for the -C=N-stretching bands at 1627 and 1635 cm^{-1} [12]. This indicated that -NH_2 group of APTES reacted with -CHO group of -Sal in condensation reaction to form imine (-C=N) and the anchoring of cobalt and manganese complexes over the amino groups of modified mesoporous silica (SBA-15) surface. There was a shift to a lower frequency, indicating the formation of a metal-Sal-APTES ligand bond [16].

Powder X-ray diffraction (XRD): X-ray diffraction diagram (XRD) of the synthesized samples are presented in Fig. 3. The results of XRD shows that three sharp diffraction peaks indexed as the (110) hkl reflections (1.05° 2θ) of the cubic $Im\bar{3}m$ group space and two small shoulder of the (200) and (211) hkl reflections (1.43 and 1.75° 2θ, respectively) [17]. All these samples have the same diffraction angles 2θ were 0.820, 0.750, 0.780 and 0.760 corresponding with the distance of d_{110} network are 109.6, 112.3, 113.5 and 111.4 Å (Table-2).

After dispersing the complex into the surface of SBA-16, the support still retained uniform mesoporous size which can

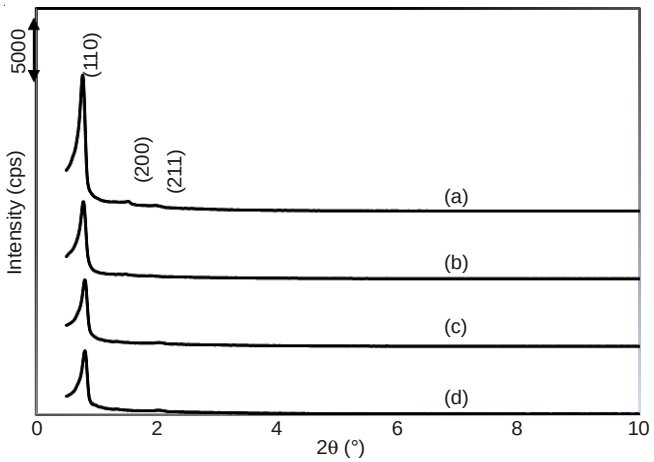

Fig. 3. XRD patterns of: (a) SBA-16, (b) Mn(II)-Sal-APTES-SBA-16, (c) Co(II)-Sal-APTES-SBA-16 and(d) Co(II)-Mn(II)-Sal-APTES-SBA-16

be seen in TEM images (Fig. 4). However the position of peak shifted to the smaller angles because the unit cell distance of d_{110} reflection increased from 0.3 to 0.4 Å. This result indicates the incorporation of the M(II)-Sal-APTES within the pore of SBA-16 by the integration of the Schiff-base complex and the silanol groups on surface of the pores [13]. The maximum peak intensity of original SBA-16 is 10,000 Cps, however for the Mn(II)-Sal-APTES-SBA-16; Co(II)-Sal-APTES-SBA-16 and Co(II)-Mn(II)-Sal-APTES-SBA-16 the highest peaks are only 5800; 5000 and 5500 Cps, respectively. Indicating the introduction of metal organic complexes into the mesoporous of SBA-16. It can be seen that the intensity of the peaks for the (200) and (211) reflections clearly decreased. The reasons

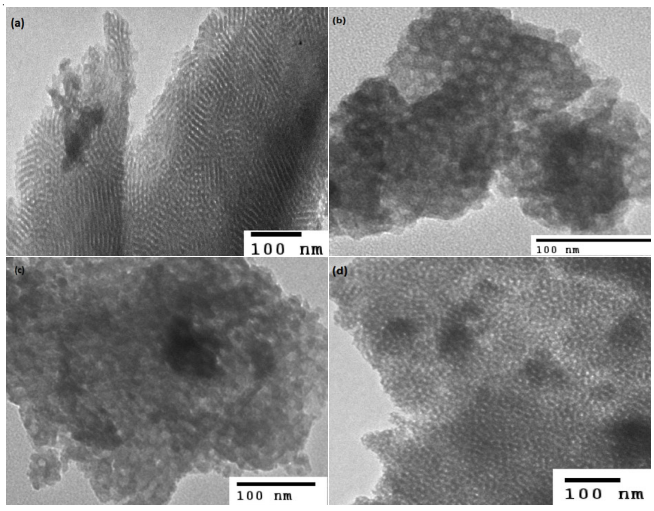

Fig. 4. TEM images of (a) Sal-SBA-16; (b) Mn(II)-Sal-APTES-SBA-16; (c) Co(II)-Sal-APTES-SBA-16 and (d) Co(II)-Mn(II)-Sal-APTES-SBA-16

TABLE-2
XRD CRYSTALLOGRAPHIC PARAMETERS OF SUPPORT AND CATALYSTS

Materials	2θ (°)	d_{110} (Å)	d_{200} (Å)	d_{211} (Å)	Intensity (cps)
SBA-16	0.82	109.6	5.80	4.46	10000
Mn(II)-Sal-APTES-SBA-16	0.78	113.5	-	-	5800
Co(II)-Sal-APTES-SBA-16	0.75	112.3	-	-	5000
Co(II)-Mn(II)-Sal-APTES-SBA-16	0.76	111.4	-	-	5500

for this would be the decrease of local order, the variation in wall thickness, or the less scattering contrast between the channel wall of the inorganic silicate framework and the organic complex of metal in the pores. These results show that the metal organic complexes have self-directed disruption of the micelle structure possessed in surfactants and silica precursors [8,13]. However, the position of the (110) hkl reflection still occurred in the same low angles, indicating that the cubic Imframework of materials was remained unchanged [17].

Transmission electron microscopy (TEM): TEM images of SBA-16; Mn(II)-Sal-APTES-SBA-16; Co(II)-Sal-APTES-SBA-16 and Co(II)-Mn(II)-Sal-APTES-SBA-16 were showed in Figs. 4a-d. The results suggesting that mesoporous silica material have highly ordered cubic mesostructure. From Figs. 4a and 4d one can clearly observe the (110) hkl reflection corresponding to cubic $Im\bar{3}m$ structure indicates that the mesoporous structure of SBA-16 was maintained after anchoring of metals complex. Figs. 4b and 4c have appearance of tiny black spots distributed onto porous channels. These TEM results are in agreement with the ordered cubic mesoprous structure obtained from the corresponding XRD results.

Nitrogen sorption isotherms: Nitrogen adsorption-desorption isotherms of SBA-16 and Co(II)-Mn(II)-Sal-APTES-SBA-16 catalyst are given in Fig. 5. It can be seen that pore volume and surface area of Co(II)-Mn(II)-Sal-APTES-SBA-16 were clearly decreased compared with the material of SBA-16 (Table-3). This would be due to the overlapping of M(II)-Sal-APTES in the mesoporous cage of the modified SBA-16. The pore entrance size of SBA-16 was the same with the molecular size of M(II)-Sal-APTES, indicating that few metal complex molecules existed inside the cages. This result is consistent with what presented in TEM images.

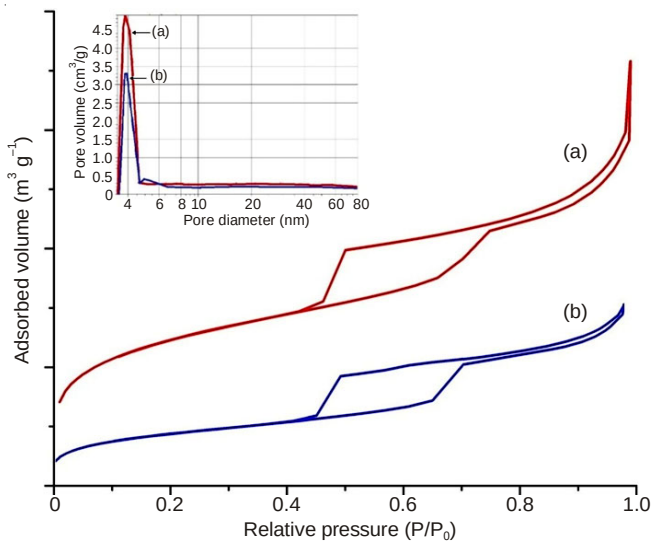

Fig. 5. Nitrogen adsorption/desorption isotherms incorporated with pore size distributions at inset of: (a) SBA-16 and (b) Co(II)-Mn(II)-Sal-APTES-SBA-16

Thermal analysis: The TGA-DTA curves of samples were analyzed in argon gas environment (Figs. 6 and 7). In TGA-DTA of APTES-SBA-16 (Fig. 6a), the TGA curve indicates an only weight loss with the exothermic peak in DTA line at 361.4 °C, which is caused by the removal of APTES. In thermogravimetric weight loss curves of the Mn(II)-Sal-APTES SBA-16 (Fig. 6b), Co(II)-Sal-APTES- SBA-16 (Fig. 6c) and Co(II)-Mn(II)-Sal-APTES-SBA-16 (Fig. 6d) showing two stages of weight loss. The first weight loss at about 370 °C is for the removal of APTES, while the second in the region of 417-460 °C is due to the decomposition of salicylaldehyde (Sal) containing benzene ring and other large molecules. These values are much higher than the boiling temperature of pure Sal and pure APTES at 760 mmHg, at (197 and 215 °C, respectively), indicating that there were a covalent bonding formation between the metal organic complex and SBA-16.

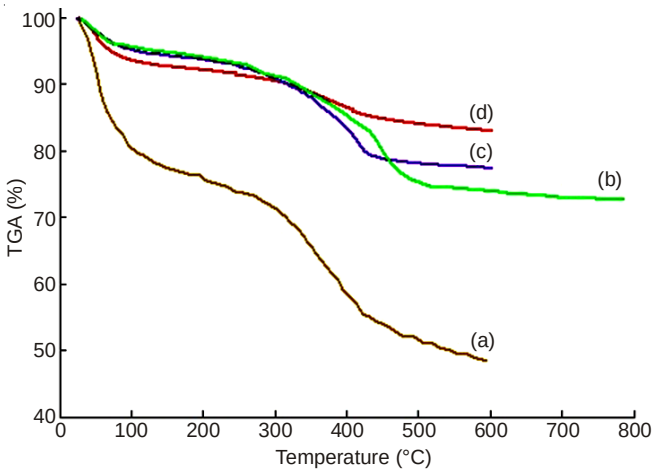

Fig. 6. Thermogravimetric analysis results of: (a)APTES-SBA-16; (b) Mn(II)-Sal-APTES-SBA-16; (c) Co(II)-Sal-APTES-SBA-16 and (d) Co(II)-Mn(II)-Sal-APTES-SBA-16

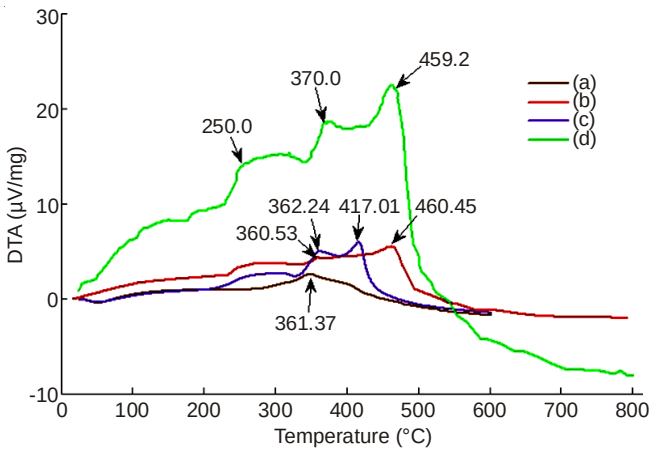

Fig. 7. DTA pattern of: (a)APTES-SBA-16; (b) Mn(II)-Sal-APTES-SBA-16; (c) Co(II)-Sal-APTES-SBA-16 and (d) Co(II)-Mn(II)-Sal-APTES-SBA-16

TABLE-3
XRD CRYSTALLOGRAPHIC PARAMETERS OF SUPPORT AND CATALYSTS

Materials	d_{110} (Å)	a_0 (Å)*	d_{pore} (Å)	S_{BET} (m^2 g^{-1})	V_{pore} (cm^3 g^{-1})
SBA-16	109.6	1.73	62	880.78	1.10
Co(II)-Mn(II)-Sal-APTES-SBA-16	111.4	1.74	77	550.50	0.54

X-ray photoelectron spectra (XPS): X-ray photoelectron spectroscopy is used to study the state of metal species on the surfaces. Fig. 8 shows the XPS spectra obtained for pure homogenous adduct of $Mn(OAc)_2$ and $Co(OAc)_2$ and Co(II)- and Mn(II)-APTES-SBA-16 (Fig. 9), intensity ratio and energy difference between the two signals obtained for electron ejected from $2p_{1/2}$ and $2p_{3/2}$ levels can be used as a tool to investigate the electronic properties of cobalt and manganese compounds. Manganese acetate compounds exhibit Mn $2p_{3/2}$ and $2p_{1/2}$ core level peaks at binding energy of 641.85 eV and 653.54 eV respectively. This result is consistent with the binding energy of the Mn-APTES complex which is immobilized into SBA-16 and has binding energies at 641.79eV and 653.42 eV, respectively [11,18]. And there are no more signals detected in the visible energy area. Therefore, we can sure that the Mn(II)-APTES complex which is immobilized into SBA-16 has oxidation state (+2) [19]. Similarly, cobalt complexes also shows an experimental trend as in Mn complexes and we obtain the result: the reported binding energy values of Co $2p_{3/2}$ peak are 779.86 eV for pure initial $Co(OAc)_2$ solution and 779.98 eV for Co-APTES complex immobilized into SBA-16 and the reported binding energy values of Co $2p_{1/2}$ peak are 795.31 eV for pure homogeneous $Co(OAc)_2$ solution and 795.09 eV for Co-APTES complex immobilized into SBA-16 [18].

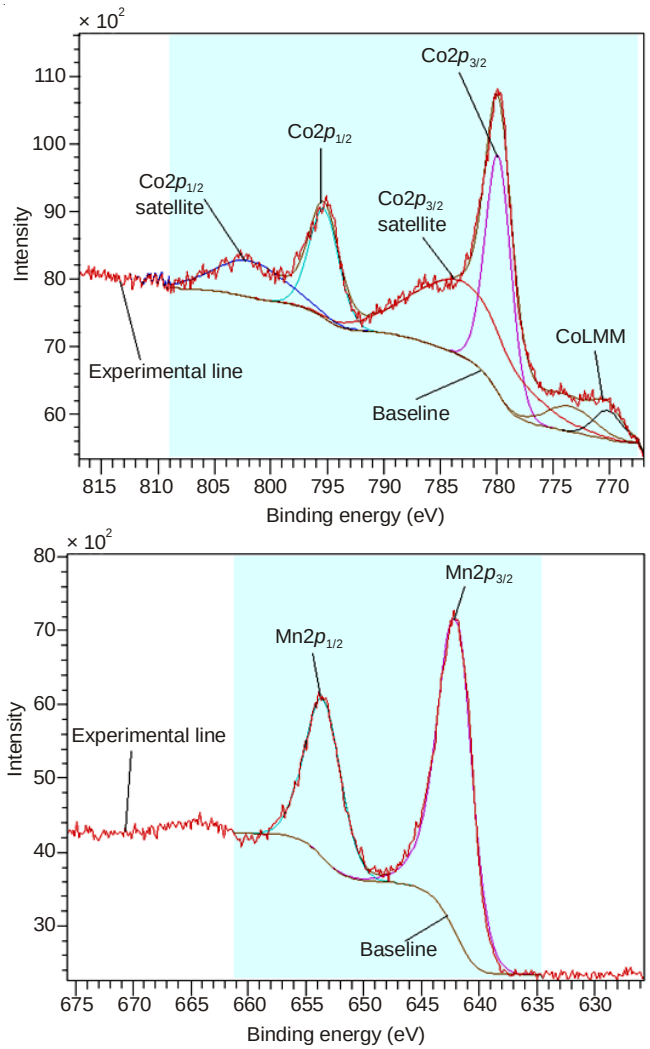

Fig. 8. XPS spectra of neat $Co(OAc)_2$ and $Mn(OAc)_2$

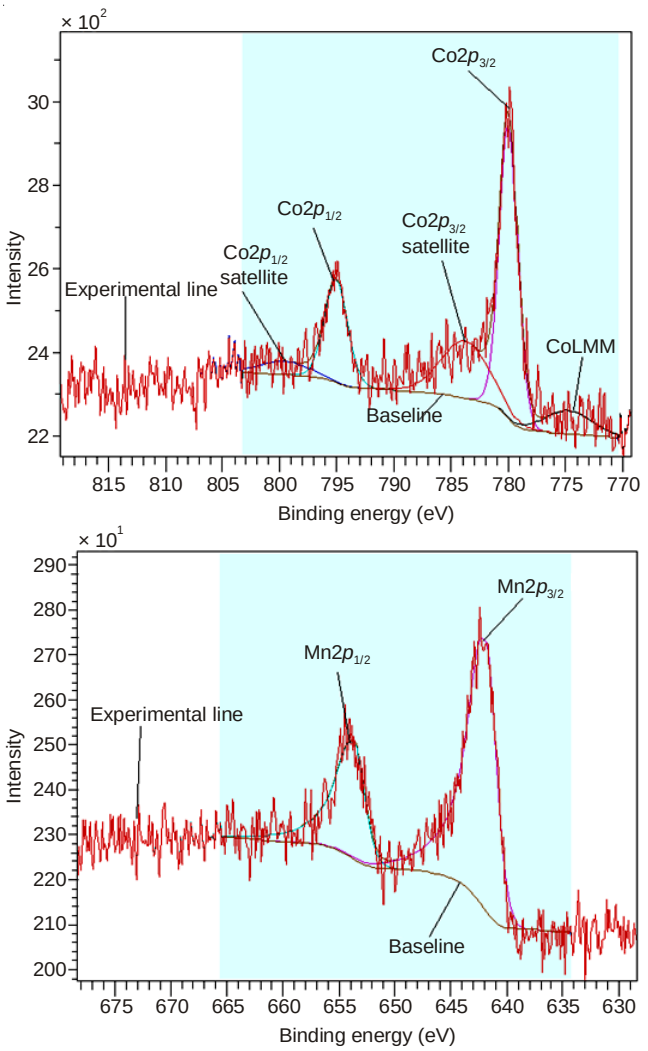

Fig. 9. XPS spectra of Co(II)-Mn(II)-Sal-APTES-SBA-16

In additional, the spectra of cobalt (II) complex also shows satellite considerable peaks at equal distances of higher than 6 eV from the corresponding main peak of Co $2p_{3/2}$, in there the ion Co (+2) (which has satellite peak) has binding energy of 782.92 eV. This result can be explained by the concept of splitting multiple spin, cobalt(II) complex has high electron-spin configuration with 3 electron undivided, therefore, exists the satellite peaks. These spectral characteristics once again help us to determine the presence of central cobalt ion in the oxidation state (+2) complex.

Catalytic activity: Oxidation reaction of *p*-xylene was carried out in liquid phase with different catalyst systems, H_2O_2 as an oxidant, a promoter KBr at 100 °C, under atmosphere pressure. The conversion and product distribution was presented in Table-4.

Under mild reaction condition (100 °C), the main products obtained in oxidation reaction of *p*-xylene such as *p*-tolylaldehyde, *p*-toluic acid, 4-carboxybenzaldehyde and terephthalic acid. Cobalt or manganese complexes immobilized SBA-16 support alone gave low conversion and *p*-tolylaldehyde was the major oxidation product. A combination of Mn(II) and Co(II) complexes were immobilized SBA-16 or the homogenous catalyst of Mn acetate and Co acetate showed the much higher conversions and higher selectivity for terephthalic acid. It

TABLE-4
OXIDATION OF *p*-XYLENE BY USING $M(OAc)_2$ AND M(II)-Sal-APTES-SBA-16 CATALYSTS

Catalyst	*p*-Xylene conversion (wt. %)	Product selectivity (wt. %)			
		p-Tolylaldehyde	*p*-Toluic acid	4-Carboxybenzaldehyde	Terephthalic acid
$Co(OAc)_2(3.0) + Mn(OAc)_2(1.0)$	99.8	56.2	17.2	10.3	16.3
Mn(3.0)-Sal-APTES-SBA-16	23.2	87.4	7.2	2.1	3.3
Co(3.0)-Sal-APTES-SBA-16	45.6	91.0	3.1	1.2	4.7
Co(3.0)-Mn(1.0)-Sal-APTES-SBA-16(C)	99.7	32.0	27.2	15.0	25.8
Co(3.0)-Mn(1.0)-Sal-APTES-SBA-16(M)	93.1	43.8	28.4	13.2	14.6

shows that occurring of cobalt and manganese are co-catalysts that enhance the catalytic activity and may be as interference in $Co/Mn/Br^-$ catalyst system with presence of H_2O_2 oxidant agent, hence, oxidation reaction of *p*-xylene follows a free radical chain mechanism [5,20,21]. Follow this mechanism Co^{3+} is formed by reaction of Co^{2+} with hydrogen peroxide in acetic acid, after that Co^{3+} reacts rapidly with Mn^{2+} to form Mn^{3+}. The Mn^{3+} ion abstracts an electron from Br^- generate the bromine radical, $Br^\bullet$, role of the $Br^\bullet$ radical is to oxidized methyl group of *p*-xylene.

It is clear that the presence of both cobalt and manganese complexes onto the SBA-16 support which was synthesized by chemically mixed complexes method have a significantly higher catalytic activity than its synthesized by mechanical mixed complexes method, its that may be homogenous interference of active metal ions phase over catalyst system. A novel finding in the study is selectivity of desirable product for terephthalic acid with metal complexes catalyst anchored silica SBA-16 support showed higher homogenous catalyst of neat metal acetate salts which may be related to the "shape selectivity" effect [22]. As indicated by N_2 sorption analysis, the synthesized SBA-16 have type of mesopore with the cubic $Im\bar{3}m$ ordered uniform pore and the diameters in the range 6.2-7.7 nm that is capable of admitting transition complexes and product [7,9]. Indeed, these pore sizes well coincide with the diameter of terephthalic acid molecule.

Conclusion

The uniform mesoporous silica SBA-16 was anchored with manganese-and cobalt-Schiff base complexes to produce metal-Schiff base-SBA-16 catalyst [Mn(II)-Sal-APTES-SBA-16 and Co(II)-Sal-APTES-SBA-16]. The manganese- and cobalt-Schiff bases were synthesized from salicylaldehyde (Sal), [(3-aminopropyl)triethoxysilane] (APTES) in ethanol and manganese acetate or cobalt acetate. Powder X-ray diffraction and transmission electron microscopy (TEM), nitrogen adsorption-desorption analyses confirm support properties was maintained after anchoring. The incorporation of Schiff-base complex matrix caused a decrease in the mesoscopic order, amount of adsorbed nitrogen, the pore volume, the specific surface area, the pore diameter and aa increase in the wall thickness. The DTA-TGA, FT-IR and XPS prove the presence of manganese- and cobalt-Schiff base complex within the pores of SBA-16.

The liquid-phase oxidation reactions of *p*-xylene with hydrogen peroxide as the oxidant were examined with these catalysts. The product selectivity of *p*-xylene oxidation using manganese-cobalt complexes was much different from using single manganese- and cobalt-complex. Especially, cobalt-manganese complexes catalysts show higher activity and selectivity than neat metal acetate salts for the oxidation reaction of methyl group under mild condition.

REFERENCES

1. K. Weissermel and H.-J. Arpe, in ed: C.R. Lindley, Industrial Organic Chemistry, VCH, New York, edn 2 (1993).
2. P.P. Rossi and M. Catoni, Process for the Preparation of ω-lactams in Particular Caprolactam, US Patent 4349473 (1980).
3. K.-T. Li and S.-W. Li, *Appl. Catal. A*, **340**, 271 (2008).
4. Y. Cheng, G. Peng, L. Wang and X. Li, *Chin. J. Chem. Eng.*, **17**, 181 (2009).
5. S.A. Chavan, S.B. Halligudi, D. Srinivas and P. Ratnasamy, *J. Mol. Catal. Chem.*, **161**, 49 (2000).
6. R. Chakrabarty, D. Kalita and B.K. Das, *Polyhedron*, **26**, 1239 (2007).
7. S.M. Islam, A.S. Roy, S. Dalapati, R. Saha, P. Mondal, K. Ghosh, S. Chatterjee, K. Sarkar, N. Guchhait and P. Mitra, *J. Mol. Catal. Chem.*, **380**, 94 (2013).
8. G.R. Bardajee, R. Malakooti, F. Jami, Z. Parsaei and H. Atashin, *Catal. Commun.*, **27**, 49 (2012).
9. C. Baleizão, B. Gigante, H. García and A. Corma, *Tetrahedron*, **60**, 10461 (2004).
10. H.S. Abbo, S.J.J. Titinchi, R. Prasad and S. Chand, *J. Mol. Catal. Chem.*, **225**, 225 (2005).
11. V.D. Chaube, S. Shylesh and A.P. Singh, *J. Mol. Catal. Chem.*, **241**, 79 (2005).
12. P. Sharma, A. Lazar and A.P. Singh, *Appl. Catal. A*, **439**, 101 (2012).
13. G.R. Bardajee, R. Malakooti, I. Abtin and H. Atashin, *Micropor. Mesopor. Mater.*, **169**, 67 (2013).
14. C.R. Jacob, S.P. Varkey and P. Ratnasamy, *Appl. Catal. A*, **182**, 91 (1999).
15. O.C. Gobin, Y. Wan, D. Zhao, F. Kleitz and S. Kaliaguine, *J. Phys. Chem. C*, **111**, 3053 (2007).
16. G. Yang, X. Chen, X. Wang, W. Xing and N. Xu, *Chin. J. Catal.*, **34**, 1326 (2013).
17. B.R. Jermy, S.-Y. Kim, K.V. Bineesh and D.-W. Park, *Micropor. Mesopor. Mater.*, **117**, 661 (2009).
18. L. Guczi, R. Sundararajan, Zs. Koppány, Z. Zsoldos, Z. Schay, F. Mizukami and S. Niwa, *J. Catal.*, **167**, 482 (1997).
19. M. Fujiwara, T. Matsushita and S. Ikeda, *J. Electron Spectrosc. Relat. Phenom.*, **74**, 201 (1995).
20. B. Saha and J.H. Espenson, *J. Mol. Catal. Chem.*, **271**, 1 (2007).
21. H. Falcon, J.M. Campos-Martin, S.M. Al-Zahrani and J.L.G. Fierro, *Catal. Commun.*, **12**, 5 (2010).
22. H. Yang, L. Zhang, W. Su, Q. Yang and C. Li, *J. Catal.*, **248**, 204 (2007).